ORIGINAL ARTICLE

New technique of radial-additive friction stir repairing for exceeded tolerance holes

Song Qi[1] · Qi Wen[1] · Shude Ji[1] · Xiangchen Meng[1] · Baosheng Wu[1] · Weiwei Qi[2]

Abstract
Radial-additive friction stir repairing (R-AFSR) was proposed to repair exceeded tolerance holes. Here, AZ31 Mg alloys were selected as the primary research object. Good metallurgical bonding appeared in the repaired zones due to atom diffusion induced by thermo-mechanical behaviors. The diameter of the exceeded tolerance hole was reduced from 10 to 8 mm. The stir zone and partial thermo-mechanically affected zone were characterized by fine and equiaxed grains. The average grain size in the stir zone was less than 10 μm, attributing to high microhardness values. A high-quality repaired joint with the maximum tensile strength of 183 MPa was achieved, equivalent to 93.8% of the joint with the standard hole for AZ31 Mg alloys. Compressive shear strength and compression rate of the repaired joint reached 58.4 MPa and 26.1%, up to 75% and 74.6% of the joint with the standard hole. The fracture surface morphologies exhibited the typical ductile fracture. Therefore, R-AFSR has great prospects to repair the exceeded tolerance holes.

Keywords Radial-additive friction stir repairing · Exceeded tolerance holes · Magnesium alloys · Microstructures · Mechanical properties

1 Introduction

Aluminum and magnesium alloys are commonly used in aerospace, automotive, shipbuilding, and other fields [1, 2]. Some defects, such as pores, inclusions, and cracks, inevitably appear in the structural parts during manufacturing and service processes, reducing the service life [3]. Currently, the repairing techniques of these defects in the metals become the research hotspots, which consist of fusion welding and solid state welding [4]. Li et al. [5] used gas tungsten arc welding (GTAW) to repair the shrinkage porosity in D357 cast aluminum alloys. Shankar et al. [6] adopted tungsten inert gas

welding (TIG) to delay the crack propagation in 5083 aluminum alloys. However, fusion welding defects, such as crack, inclusion, pore, and segregation, easily occur in the repaired region, reducing mechanical properties severely [7].

As a solid state welding technique, friction stir welding (FSW) has the advantage of high joint quality, small distortion, low residual stress, and non-pollution [8–12]. Therefore, FSW has been widely applied in aviation and other manufacturing fields [13]. Friction stir repairing (FSR), a repairing technique derived from FSW, has attracted extensive attentions. Many repairing techniques were investigated by scholars, including vertical compensation FSW [14–16], re-FSW [17], friction taper plug welding (FTPW) [18], friction plug welding (FPW) [19], friction bit joining (FBJ) [20], friction flow welding (FFW) [3], and active-passive filling friction stir repairing (A-PFFSR) [21, 22]. These methods are divided into two categories: extra filling material (FM) repairing and non-filling material repairing.

For the non-filling material repairing, Ren et al. [23] used the re-FSW to repair the cracks in 2024 aluminum alloys. Liu et al. [24] employed re-FSW to repair groove defects in FSW joints. Zhou et al. [25] studied a self-refilling friction stir welding (SRFSW), during which the keyhole defect was refilled using the materials around the keyhole step by step.

Song Qi and Qi Wen contributed equally to this work.

✉ Shude Ji
  superjsd@163.com

✉ Xiangchen Meng
  mengxch2013@163.com

1 School of Aerospace Engineering, Shenyang Aerospace University, Shenyang 110136, China

2 Liaoning Dralong Unmanned Aerial Vehicle Technology Co.,Ltd., Shenyang 110036, China

For the volume defects, the extra FM is necessary. A consumable rotating pin as an extra FM was added during the FPTW and FJB processes. Huang et al. [26] put forward filling friction stir welding (FFSW), and a semi-consumable tool consisted of a consumable rotating pin and a non-consumable rotating shoulder. In fact, when the consumable pin acted as the extra FM, the kissing bond defect is difficult to be eliminated because of insufficient frictional heat [27]. In order to solve the abovementioned problems, Ji et al. [21, 22] proposed A-PFFSR by a series of pinless tools with different shoulder diameters to repair the keyhole defects with arbitrary depths.

Currently, wear and corrosion in metallic structures during long period service easily result in exceeded tolerance holes, reducing service life and mechanical properties. Although exceeded tolerance holes are repaired by solid-state repairing methods, a re-drilling process is still essential. In this study, a novel repairing technique named radial-additive friction stir repairing (R-AFSR) was proposed by a non-consumable rotating tool and an extra FM. Meanwhile, joint formation, microstructures, and mechanical properties of repaired regions were mainly investigated in detail.

2 Experimental procedures

2.1 R-AFSR process

Figure 1 indicates the schematic of the R-AFSR process. A rotating tool was composed of a threaded cylindrical pin and a concave concentric-circles-flute shoulder. The FM and base metal (BM) were heterogeneous. The R-AFSR process included the drilling, filling, repairing, and retracting stages. A pinless tool and a cylindrical right-handed thread pin tool were used. Firstly, a pinless tool was plunged into the workpiece, thereby obtaining a cylinder-shaped hole (Fig. 1a). Secondly, the FM was put into the hole before the repairing process (Fig. 1b). Thirdly, the rotating tool was gradually plunged into the workpiece to a designed depth and dwelled for a few seconds (Fig. 1c). Finally, the exceeded tolerance hole was repaired after the rotating tool was retracted, obtaining high-quality repairing interfaces (Fig. 1d).

In the previous studies, FTPW, FBJ, FFSW, A-PFFSR, and drilling-filling FSR (D-FFSR) could repair the exceeded tolerance hole by means of completely filling the holes. However, two problems exist at these techniques. On one hand, after the exceeded tolerance hole was successfully filled, the repaired region was machined into a standard hole to perform the metallurgical joining. On the other hand, kissing bond defects easily existed at the joining interface because the deformable rotating pin produced insufficient frictional heat and low forging pressure. The R-AFSR process can solve these problems because the non-deformable rotating pin was used.

2.2 Materials

The BM was AZ31 Mg alloy plates, whose dimensions were 200 mm × 200 mm × 3 mm. The repairing experiments were performed by the FSW-3LM-4012 machine. A tilting angle relative to Z-axis was 0. Before the R-AFSR process, the top surface of the AZ31 Mg plate and the outer surface of the FM were polished with emery paper to wipe off oxide layers. A pinless tool with a six-spiral-flute shoulder and a diameter of 10 mm was beneficial to obtaining a flat hole bottom and facilitating material filling. A rotating tool with a cylindrical right-handed thread pin was used to repair the defects. The shoulder diameter, pin length, and pin diameter were 14 mm, 2.8 mm, and 8 mm, respectively. A hole with a depth of 2.5 mm was drilled by the six-spiral-flute pinless tool. The height of the FM was 0.5 mm higher than the depth of the drilled hole to eliminate thickness reduction. A plunge speed of 2 mm/min and a dwelling time of 20 s were fixed. The rotating velocities were 1200 rpm, 1400 rpm, and 1600 rpm, correspondingly.

2.3 Characterization

The specimens after repairing were cut by an electrical discharge cutting machine to conduct microstructural and mechanical characterizations (Fig. 2). The microstructural specimens were etched by picric acid (4.2 g picric acid, 10 ml H_2O, 10 ml acetic acid, and 70 ml ethanol) and then observed by an optical microscope (OLYMPUS, GX71) and scanning electron microscope (SEM, HITACH-SU3500). To evaluate the mechanical properties of R-AFSR holes, two mechanical testing methods were used, including tensile tests and compressive shear tests. Three tensile specimens were prepared for each parameter with reference to GB/T2651-2008 (ISO 4136:2011). Schematic of the tensile specimen is presented in Fig. 2b. In addition, the repaired region was filled with a mandrel before tensile tests. Tensile tests at room temperature were performed under a constant crosshead speed of 3 mm/min. In this study, the standard hole and the repaired region were investigated for tensile tests, and these holes had the same diameter. Moreover, a self-designed compressive shear apparatus is shown in Fig. 3a, and the sample is presented in Fig. 2c. The compressive shear strength formula is $P=F/S$, where F is compressive shear force (N) and S is compressive shear area (m^2). Fracture surface morphologies of tensile specimens were observed by a SEM (HITACH-SU3500). The microhardness of the repaired region was measured by the microhardness tester (HVS-1000) at a load of 100 g for a dwelling time of 10 s. The measured locations were 0.5 mm and 1.5 mm distances away from the top surface of the repaired region, and the interval between the two measured points was 0.25 mm (Fig. 3b).

Fig. 1 Schematic of R-AFSR: (a) drilling, (b) filling, (c) repairing, and (d) retracting stages
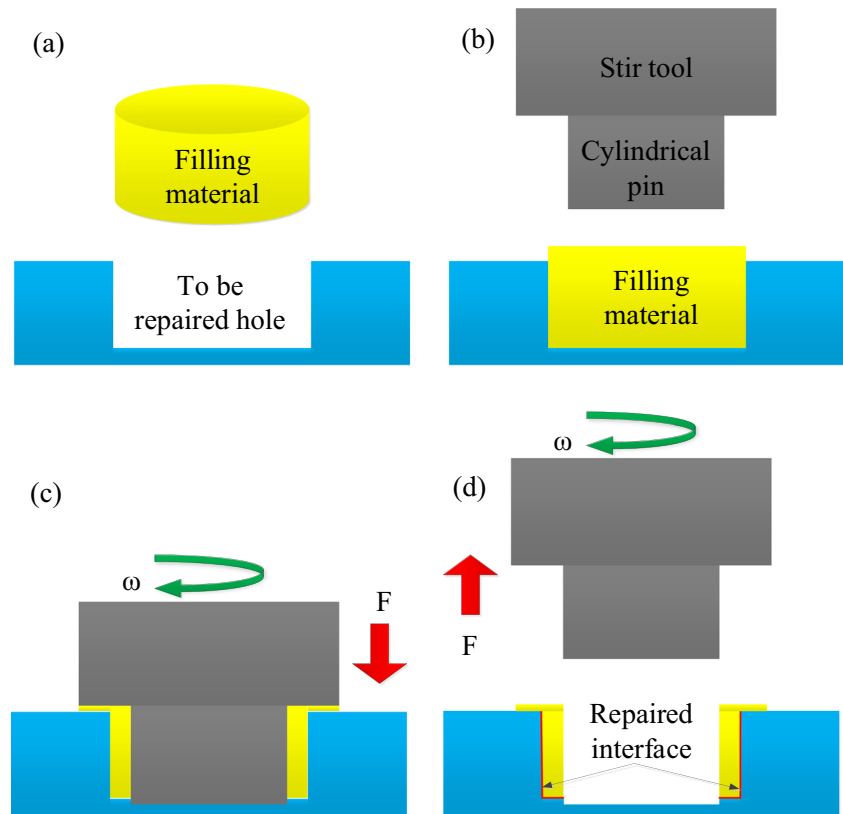
3 Results and discussion

3.1 Material flow

For the R-AFSR process, material flow behaviors at the drilling and repairing stages are very important. At the drilling stage, the pinless tool rotates anticlockwise to extrude out of the material, forming a hole. The material flow behavior at this stage is the same as that reported by Ji et al. [22]. However, the rotating direction of the tool at the repairing stage should be clockwise rather than anticlockwise, which is thoroughly discussed as follows.

Figure 4a and b displays the material flow models at the repairing stage when the tool rotates anticlockwise and clockwise, respectively. At the repairing stage, the threaded pin drives the plastic materials to vertically flow. The materials in the threaded grooves undergo two forces, which are the positive pressure (p) provided by the side wall of threaded grooves and the friction force (f) between the plasticized materials and the side wall of threaded grooves. The resultant
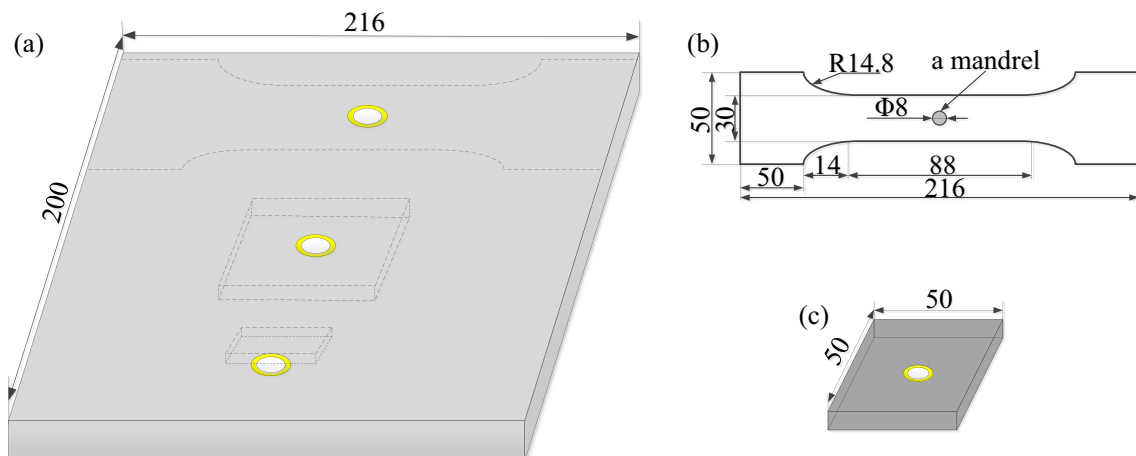
Fig. 2 Schematics of mechanical specimens: (a) testing plate, (b) tensile sample, and (c) compressive shear sample (unit, mm)
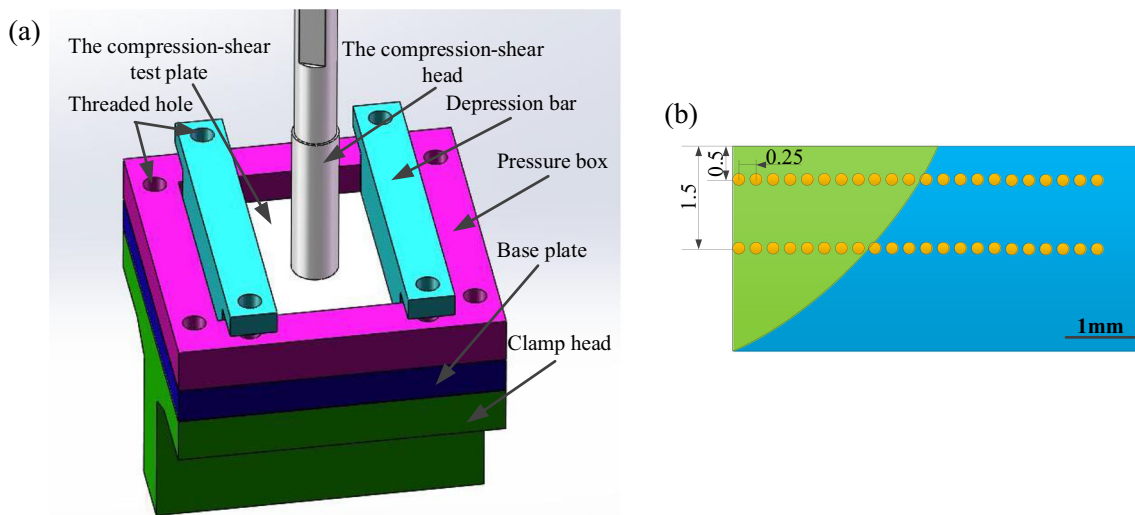
Fig. 3 Schematics: (a) compressive shear apparatus and (b) locations of the measured points for hardness (unit, mm)

force between p and f dominates the flow direction of the plasticized materials around the rotating pin. In this study, the right-handed thread pin transfers the materials downward or flow upward when it rotates anticlockwise or clockwise (Fig. 4a and b). In Fig. 4a, much more materials are accumulated around the pin tip, forming material accumulated zone (MAZ). The MAZ pushes the FM between the pin and the BM to move upward, which is detrimental to the atom diffusion bonding between the FM and the BM. Moreover, not only does the tool shoulder prevent the FM between the pin and the BM from flowing upward, but also the continuously plunging shoulder drives the materials to transfer downward. Therefore, when the right-handed thread pin rotates anticlockwise, kissing bond easily appears in the center of the stir zone

(SZ) or the bottom near the boundary between the FM and the BM (Fig. 4c). When the rotating tool rotates clockwise, the materials driven by the pin flow upward, thereby forming the MAZ beneath the tool shoulder (Fig. 4b). The materials in the MAZ are driven to flow downward, and then provide big force on the FM, which is beneficial to improving the atom diffusion. Therefore, for the R-AFSR process, the defect-free repaired region can be attained when the tool pin rotates clockwise.

3.2 Surface morphologies

Figure 5 depicts the surface morphologies of the repaired regions at different stages. In Fig. 5a, a cylinder-shaped hole with a depth of 2.5 mm is obtained by the rotating pinless
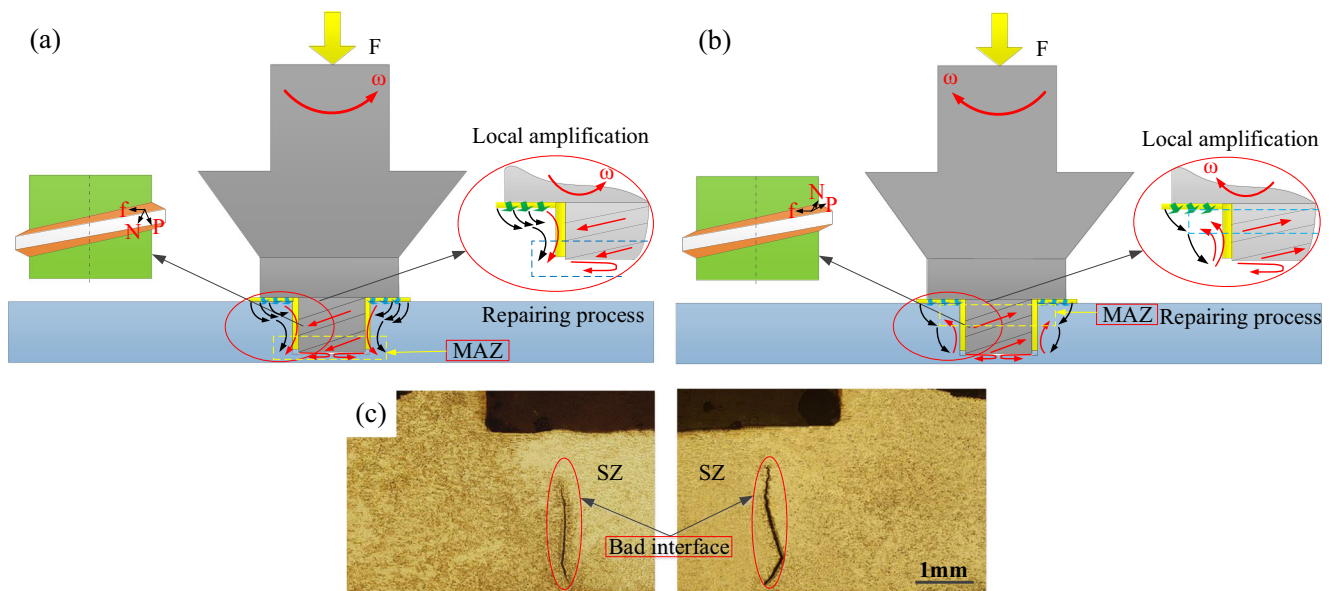
Fig. 4 Schematics of material flow at the repairing stage under different rotating directions: (a) anticlockwise and (b) clockwise; (c) cross-sections of the repaired regions at anticlockwise
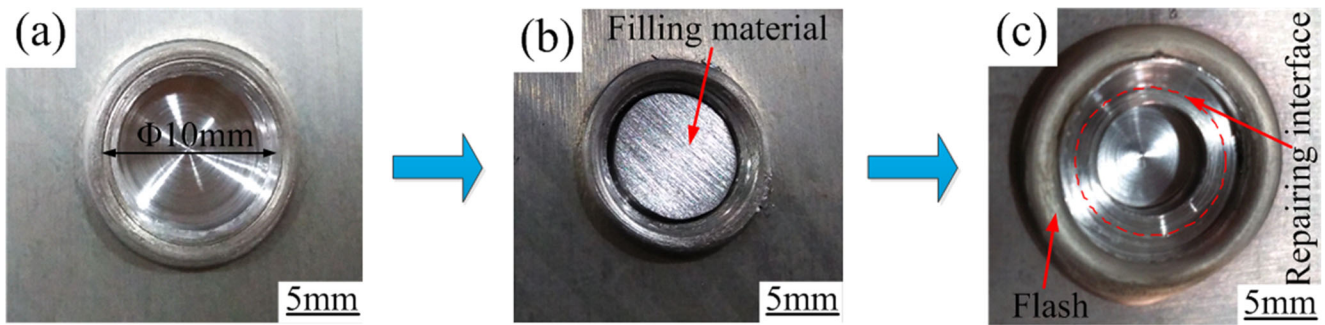
Fig. 5 Surface morphologies at different stages at a rotating velocity of 1400 rpm: (a) drilling stage, (b) filling stage, and (c) retracting stage

tool. At the drilling stage, the flash defects are formed around the repaired region because some materials are squeezed out. At the filling stage, an extra FM with a diameter of 10 mm is put into the hole, as presented in Fig. 5b. The repaired region after the retracting stage is displayed in Fig. 5c. The gap between the FM and the BM is completely filled and repaired. The hole with a diameter of 10 mm is transformed into a hole with a diameter of 8 mm by the cylindrical right-threaded pin. At the repairing stage, the tool pin is plunged into the FM and extrudes the materials out of the repairing zone, further enlarging the flashes around the hole. Therefore, compared with the flashes in Fig. 5a or b, the flash in Fig. 5c at the retracting stage is larger. Based on good surface formation of the repaired region (Fig. 5c), it is concluded that the R-AFSR process has potential to repair the exceeded tolerance hole.

3.3 Microstructures

Figure 6 presents the macrostructures of the repaired regions at the rotating velocities of 1200 rpm, 1400 rpm, and 1600 rpm, correspondingly. The exceeded tolerance hole can be successfully repaired. The repaired region is divided into four typical zones, namely, BM, heat-affected zone (HAZ), thermo-mechanically affected zone (TMAZ), and SZ, as shown in Fig. 6a. The SZ presents a funnel shape, resulting from the combined actions of the rotating pin and shoulder. The repaired interface displays a black line in Fig. 6a due to severe thermo-mechanical flow, which is composed of fine and equiaxed grains. As the rotating velocity increases, the black line is gradually narrowed. Moreover, the repaired region without thickness reduction is successfully attained,

Fig. 6 Macrostructures of the repaired regions under different rotating velocities: (a) 1200 rpm, (b) 1400 rpm, and (c) 1600 rpm
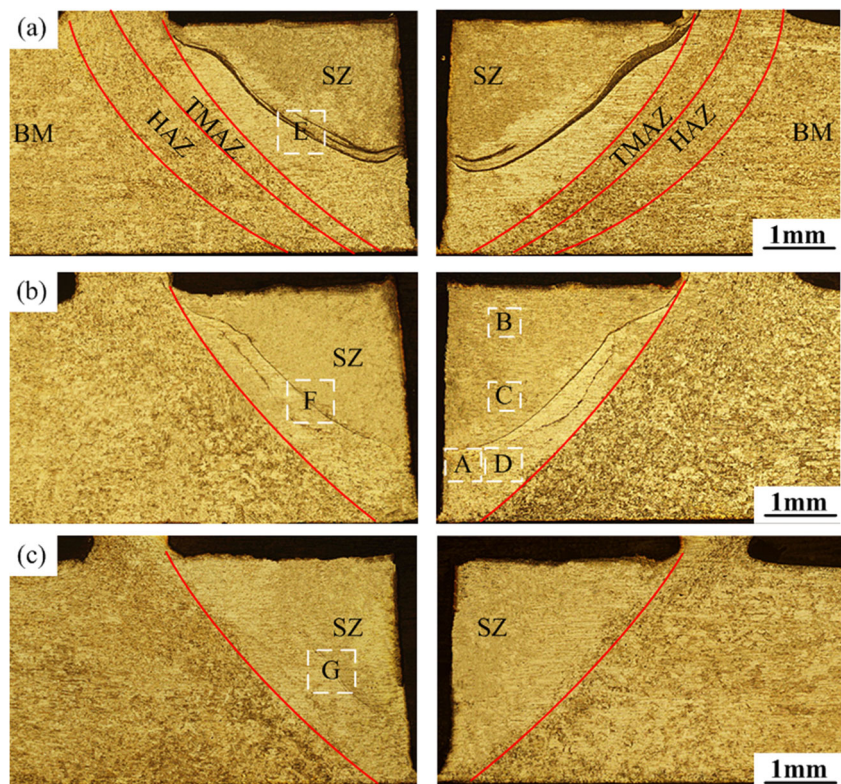
Fig. 7 Microstructures of the typical zones in the repaired region at the rotating velocity of 1400 rpm: (a) BM, (b) HAZ, (c) TMAZ, and (d) black line
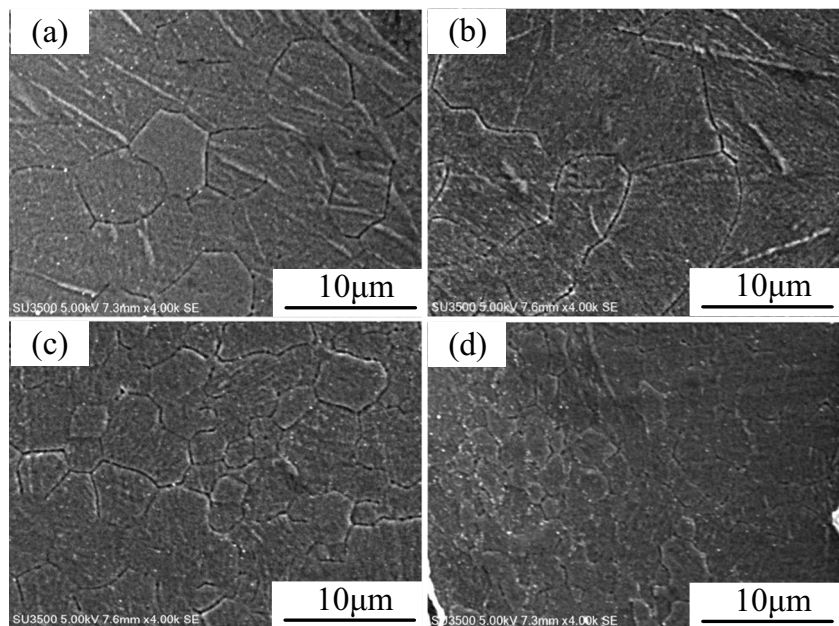
which increases the area of load bearing and improves mechanical properties. The FM and the BM near the rotating shoulder are sufficiently mixed at the repairing stage, so there is no black line near the top surface of the repaired regions (Figs. 6a and b). With the increase of rotating velocity, the materials experience higher temperature, which easily result in the growth of the fine grains. This is the reason why the black line in Fig. 6c disappears at the rotating velocity of 1600 rpm.

Figure 7 illustrates the microstructures at the BM, HAZ, and TMAZ of the typical joint. The microstructures in the BM present inhomogeneous grains (Fig. 7a). The materials in the HAZ only undergo the thermal cycle, resulting in the coarse grains. During the R-AFSR process, the temperature in TMAZ is higher than that in HAZ because the materials in the TMAZ undergo both the thermal cycle and the mechanical stirring. Therefore, the TMAZ of the repaired region for Al alloys is characterized by the elongated and deformed grains. Compared with Al alloys, Mg alloys own low stacking fault energy and low recrystallization temperature. Consequently, dynamic recrystallization (DRX) easily occurs in the TMAZ of FSW or FSR process of Mg alloys [28]. In this study, the microstructures in the TMAZ in Fig. 7c are featured by the fine and equiaxed grains, which are much smaller than those in the BM. Moreover, compared with the BM, HAZ,

Fig. 8 Microstructures of typical locations marked in Fig. 6b: (a) A, (b) B, (c) C, and (d) D
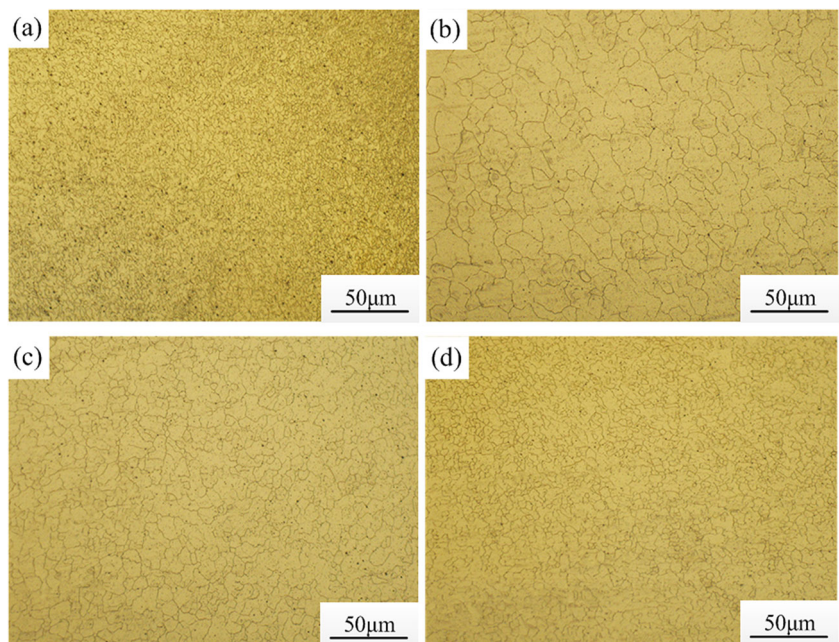
Fig. 9 Microstructures of the repaired interfaces in Fig. 6 under different rotating velocities: (a) E, (b) F, and (c) G
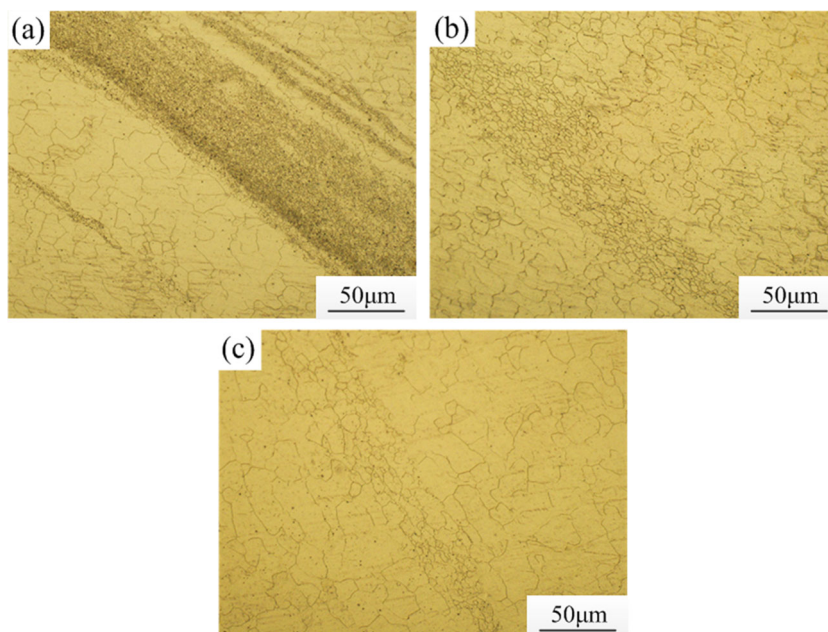
and TMAZ, the grain in the black line is formed by the finer grains (Fig. 7c), which is because of the severe thermo-mechanical flow.

Figure 8 displays the microstructures of typical locations in the SZ at 1400 rpm. The SZ is characterized by the fine and equiaxed grains owing to the DRX induced by high peak temperature and strain rate [29]. As mentioned above, the materials contacting with the rotating pin possess the high flow velocity, and the adjacent materials undergo the flow velocity that decreases with increasing the distance from the pin. Therefore, the grain size in the SZ increases with distancing away from the repaired region due to the differences in peak temperature and material flow behavior. The grain sizes in locations A and D are, respectively, 3.5 μm and 6.5 μm (Figs. 6a and b). Along the thickness direction, the materials in the top of the SZ experience higher flow velocity and peak temperature than those in the middle or bottom of the SZ because

of the rotating shoulder. Consequently, the grain size in location D is smaller than that in location C. The grain size in location C is 8.6 μm. The grain size of 9.9 μm in location B is the largest.

As mentioned above, there exist some black lines in the SZ (Fig. 6). In order to explicit these lines, the enlarged views of the typical locations are displayed, as shown in Fig. 9. These black lines contain amounts of fine grains. As the grain size decreases, the line becomes black. Niu et al. [30] put forward passive-filling friction stir repairing (P-FFSR) of AZ31-B magnesium alloys and found that a large number of fine grains existed at the interface between the extra FM and the BM. In this study, the phenomenon in Fig. 9 is similar to that reported by Niu et al. [30], which is also contributed to the grinding process between the FM and the BM. For the R-AFSR process, the heat input increases with increasing rotating velocity, thereby heightening the peak temperature and increasing the growth of grains. Therefore, the grains, which form the black line, have the increasing size with the raise of rotating velocity, leading to the reduction of black line (Fig. 9). From Figs. 8 and 9, it is also known that the top of the SZ consists of the grains with larger sizes and the grain size increases with the raise of heat input, which is another reason why the top of the SZ in Fig. 6c has no black lines.

3.4 Microhardness

Figure 10 displays the distribution curves in grain size from the SZ to BM. The grain size increases firstly and then decreases from the SZ to BM, while the grain size in the HAZ is the largest. Figure 10 displays the microhardness distribution
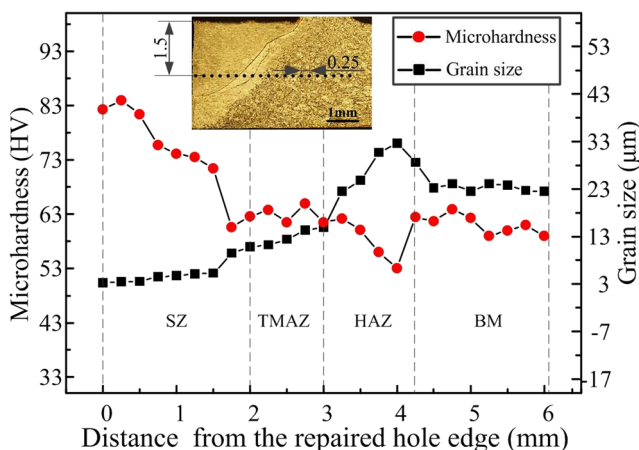
Fig. 10 Grain size and microhardness distributions of the typical repaired region
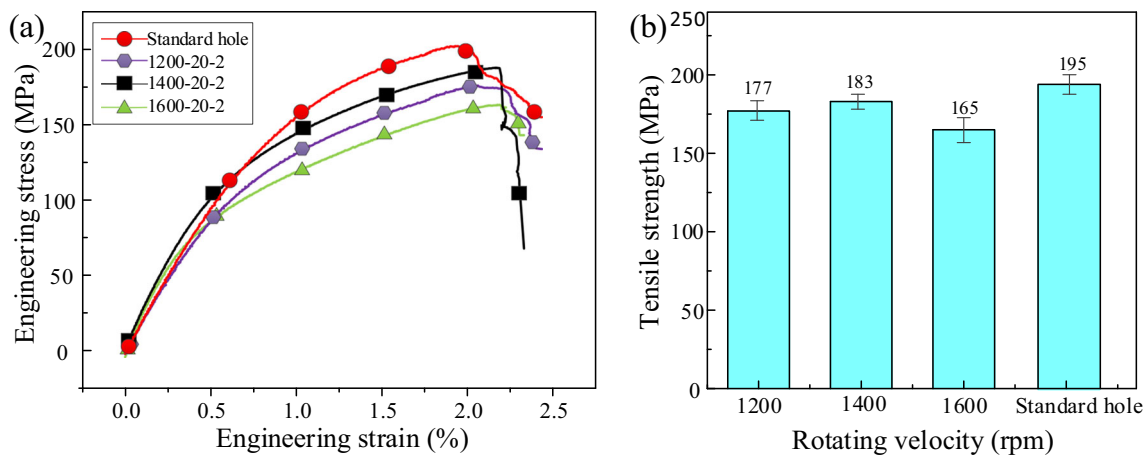
Fig. 11 Tensile results of the repaired regions: (a) engineering stress-strain curves, (b) tensile strength

of the repaired region at 1400 rpm. Two measured lines are, respectively, 0.5 mm and 1.5 mm away from the top surface of the repaired region. Both of the lines have the similar distribution. According to the Hall-Petch formula, the finer the grain size, the higher the microhardness. The grains in the SZ are greatly refined by the rotating tool, so the microhardness values in the SZ are higher than those in other regions. The HAZ consists of the coarse grains, so the microhardness values in the HAZ are the smallest.

3.5 Tensile and compressive properties

Figure 11a and b exhibits the engineering stress-strain curves and ultimate tensile strengths of the repaired regions at different rotating velocities, correspondingly. The ultimate tensile strength of the standard hole is approximately 195 MPa. The ultimate tensile strengths of the repaired regions firstly increase and then decrease with the increase in the rotating velocity. Moreover, the ultimate tensile strength of the superior repaired region reaches the maximum value of 183 MPa at

1400 rpm, which is equivalent to 93.8% of that of the standard hole. The tensile strength of the repaired region is improved when the rotating velocity varies from 1200 rpm to 1400 rpm. However, the tensile strength decreases when the rotating velocity increases from 1400 rpm to 1600 rpm. This reduction of tensile strength is attributed to the softening regions induced by the heat input and interfacial defects. Therefore, selecting reasonable process parameters is extremely essential for the R-AFSR process to obtain the high-quality repaired regions.

Figure 12 displays the compressive shear strengths and compressive rates of the repaired regions at different rotating velocities. Rotating velocity plays an important role in compressive shear strengths and compressive rates. With the increase of rotating velocity, both compressive shear strengths and compressive rates of repaired regions firstly increase and then decrease. Similar to the tensile strength, the compressive shear strength and compressive rate of the repaired region reach the maximum values of 58.4 MPa and 26.1% at the rotating velocity of 1400 rpm, equivalent to 75% and 74.6% of those of the standard hole. As a matter of fact, the

Fig. 12 Compressive shear strengths and compression rates at different rotating velocities
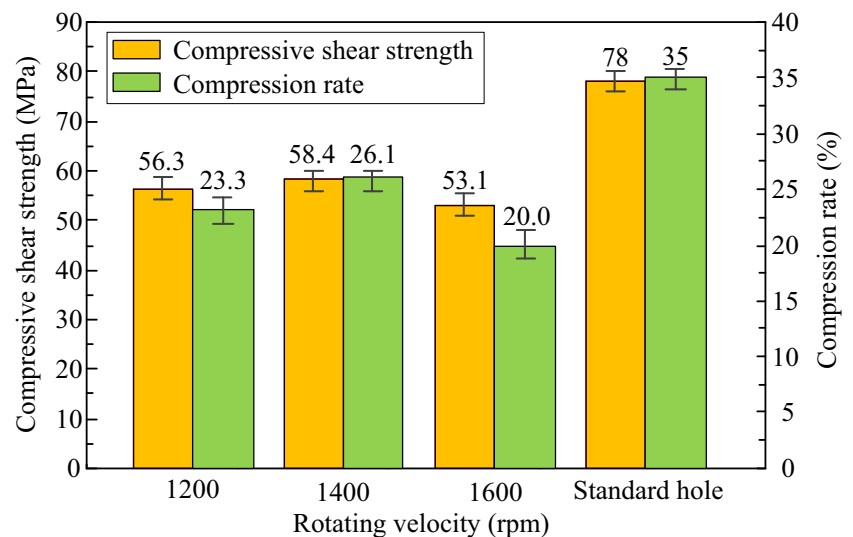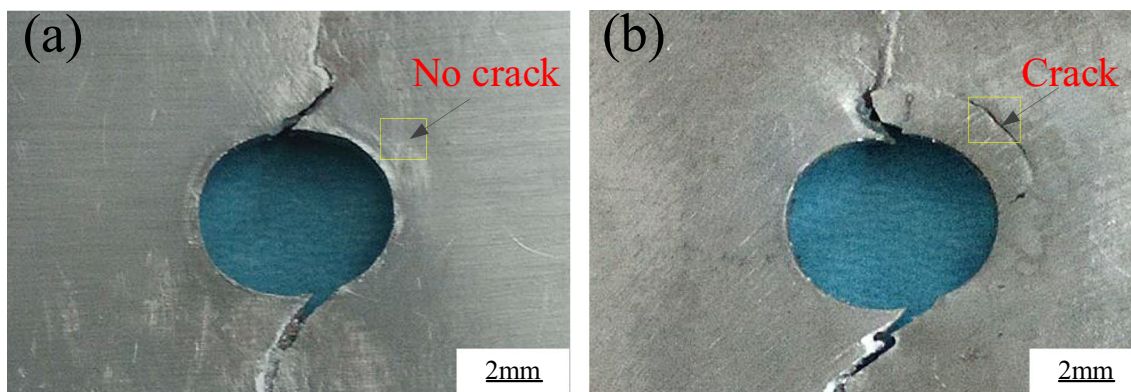
Fig. 13 Enlarged views of fractured tensile samples under different rotating velocities: (a) 1400 rpm and (b) 1600 rpm

compressive shear strength of the repaired region is closely related to interfacial behaviors and heat input. The atomic diffusion near the joining interface is an important factor. In addition, low heat input causes poor material flow, leading to the formation of interfacial defects. High heat input causes material softening, thereby deteriorating mechanical properties. When optimum heat input is achieved, the best mechanical properties can be obtained in the repaired region.

3.6 Fracture characteristics

Figure 13 displays the fracture surface morphologies of the tensile fractured samples at 1400 rpm and 1600 rpm. The crack appears near the interface between FM and BM of the repaired region at 1600 rpm rather than 1400 rpm, which verifies that the interfacial bonding strength at 1600 rpm is much lower than that at 1400 rpm. Figure 14 displays the fracture surface morphologies of the standard and repaired regions after tensile tests. The fracture locations at different

rotating velocities are all the same. The fracture surface of the standard hole (Fig. 14) is characterized by the dimples with several tearing ridges, exhibiting the typical ductile fracture. Moreover, the other samples at different rotating velocities present the similar fracture surface morphologies containing the dimples with varied size and depth (Fig. 14b–d), indicating the typical ductile fracture and good metallurgical bonding.

4 Conclusions

The R-AFSR technique was proposed to repair the exceeded tolerance hole caused by wear and corrosion during long service in practical engineering applications. The following conclusions were drawn based on the present investigation.

(1) The R-AFSR technique was successfully used to repair the exceeded tolerance hole based on the atom diffusion induced by severe thermo-mechanical behaviors.

Fig. 14 Fracture surface micrographs of tensile fractured samples: (a) standard hole; repaired regions: (b) 1200 rpm, (c) 1400 rpm and (d) 1600 rpm
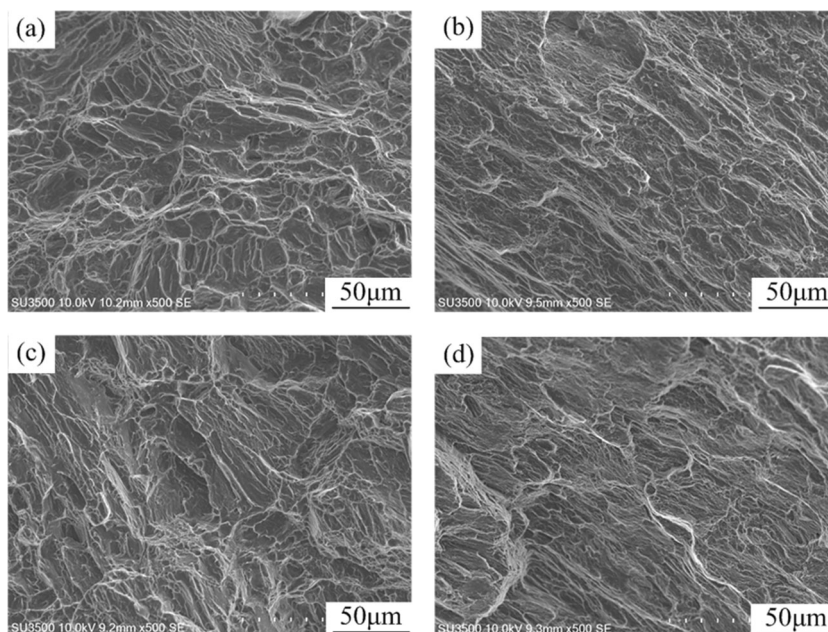
Excellent repaired regions without thickness reduction were attained at wide process window.

(2) Kissing bond defect disappeared at the interface between the FM and the BM under optimum process parameters. The SZ was characterized by fine and equiaxed grains, thereby resulting in the high microhardness values.

(3) The tensile strength of the repaired region firstly increased and then decreased. The tensile strength of the superior repaired region reached 183 MPa at 1400 rpm, which was equivalent to 93.8% of that of the standard hole. Moreover, the compressive shear strength and compressive rate of the repaired region reached 58.4 MPa and 26.1% at 1400 rpm, equivalent to 75% and 74.6% of those in the standard hole. The fracture surface morphologies of the repaired region exhibited the typical ductile fracture.

(4) The R-AFSR has feasibility and huge potential in repairing the exceeded tolerance hole based on the advantages of low peak temperature, high repairing quality, large load bearing area, simple process, high adaptability, and so on.

References

1. Meng X, Xu Z, Huang Y, Xie Y, Wang Y, Wan L, Lv Z, Cao J (2018) Interface characteristic and tensile property of friction stir lap welding of dissimilar aircraft 2060-T8 and 2099-T83 Al–Li alloys. Int J Adv Manuf Technol 94:1253–1261. https://doi.org/10.1007/s00170-017-0996-4

2. Guan M, Wang Y, Huang Y et al (2019) Non-weld-thinning friction stir welding. Mater Lett 255:126506. https://doi.org/10.1016/j.matlet.2019.126506

3. Huang R, Ji S, Meng X, Li Z (2018) Drilling-filling friction stir repairing of AZ31B magnesium alloy. J Mater Process Technol 255:765–772. https://doi.org/10.1016/j.jmatprotec.2018.01.019

4. Kim YG, Fujii H, Tsumura T et al (2006) Three defect types in friction stir welding of aluminum die casting alloy. Mater Sci Eng A 415:250–254. https://doi.org/10.1016/j.msea.2005.09.072

5. Li L, Liu Z, Snow M (2006) Effect of defects on fatigue strength of GTAW repaired cast aluminum alloy. Weld J 85:264

6. Shankar K, Wu W (2002) Effect of welding and weld repair on crack propagation behaviour in aluminium alloy 5083 plates. Mater Des 23:201–208. https://doi.org/10.1016/S0261-3069(01)00059-0

7. Tu JF, Paleocrassas AG (2011) Fatigue crack fusion in thin-sheet aluminum alloys AA7075-T6 using low-speed fiber laser welding. J Mater Process Technol 211:95–102. https://doi.org/10.1016/j.jmatprotec.2010.09.001

8. Huang Y, Meng X, Xie Y et al (2018) Friction stir welding/processing of polymers and polymer matrix composites. Compos A Appl Sci Manuf 105:235–257. https://doi.org/10.1016/j.compositesa.2017.12.005

9. Huang Y, Huang T, Wan L et al (2019) Material flow and mechanical properties of aluminum-to-steel self-riveting friction stir lap joints. J Mater Process Technol. https://doi.org/10.1016/j.jmatprotec.2018.08.011

10. Huang Y, Xie Y, Meng X et al (2018) Numerical design of high depth-to-width ratio friction stir welding. J Mater Process Technol 252:233–241. https://doi.org/10.1016/j.jmatprotec.2017.09.029

11. Huang Y, Wang Y, Wan L et al (2016) Material-flow behavior during friction-stir welding of 6082-T6 aluminum alloy. Int J Adv Manuf Technol 87:1115–1123. https://doi.org/10.1007/s00170-016-8603-7

12. Zhou L, Li GH, Liu CL, Wang J, Huang YX, Feng JC, Meng FX (2017) Effect of rotation speed on microstructure and mechanical properties of self-reacting friction stir welded Al-Mg-Si alloy. Int J Adv Manuf Technol 89:3509–3516. https://doi.org/10.1007/s00170-016-9318-5

13. Xu WF, Luo YX, Fu MW (2018) Microstructure evolution in the conventional single side and bobbin tool friction stir welding of thick rolled 7085-T7452 aluminum alloy. Mater Charact 138:48–55. https://doi.org/10.1016/j.matchar.2018.01.051

14. Ji S, Meng X, Ma L et al (2015) Vertical compensation friction stir welding assisted by external stationary shoulder. Mater Des 68:72–79. https://doi.org/10.1016/j.matdes.2014.12.009

15. Ji SD, Meng XC, Li ZW, Ma L, Gao SS (2016) Investigation of vertical compensation friction stir-welded 7 N01-T4 aluminum alloy. Int J Adv Manuf Technol 84:2391–2399. https://doi.org/10.1007/s00170-015-7904-6

16. Ji S, Meng X, Xing J et al (2016) Vertical compensation friction stir welding of 6061-T6 aluminum alloy. High Temp Mater Process 35:843–851. https://doi.org/10.1515/htmp-2015-0063

17. Liu H, Zhang H (2009) Repair welding process of friction stir welding groove defect. Trans Nonferrous Metals Soc China 19:563–567. https://doi.org/10.1016/S1003-6326(08)60313-1

18. Cui L, Yang X, Wang D et al (2014) Friction taper plug welding for S355 steel in underwater wet conditions: welding performance, microstructures and mechanical properties. Mater Sci Eng A 611:15–28. https://doi.org/10.1016/j.msea.2014.04.087

19. Du B, Sun Z, Yang X et al (2016) Characteristics of friction plug welding to 10 mm thick AA2219-T87 sheet: Weld formation, microstructure and mechanical property. Mater Sci Eng A 654:21–29. https://doi.org/10.1016/j.msea.2015.12.019

20. Lim YC, Squires L, Pan TY et al (2015) Study of mechanical joint strength of aluminum alloy 7075-T6 and dual phase steel 980 welded by friction bit joining and weld-bonding under corrosion medium. Mater Des 69:37–43. https://doi.org/10.1016/j.matdes.2014.12.043

21. Ji SD, Meng XC, Huang RF et al (2016) Microstructures and mechanical properties of 7 N01-T4 aluminum alloy joints by active-passive filling friction stir repairing. Mater Sci Eng A 664. https://doi.org/10.1016/j.msea.2016.03.131

22. Ji S, Meng X, Zeng Y et al (2016) New technique for eliminating keyhole by active-passive filling friction stir repairing. Mater Des 97:175–182. https://doi.org/10.1016/j.matdes.2016.02.088

23. Ren J-G, Wang L, Xu D-K, Xie LY, Zhang ZC (2017) Analysis and modeling of friction stir processing-based crack repairing in 2024 aluminum alloy. Acta Metall Sin 30:228–237. https://doi.org/10.1007/s40195-016-0489-8

24. Liu HJ, Zhang HJ (2012) Study of hybrid welding repair process of friction stir welding grove defect. Sci Technol Weld Join 17:169–173. https://doi.org/10.1179/136217111X13218932822646

25. Zhou L, Liu D, Nakata K et al (2012) New technique of self-refilling friction stir welding to repair keyhole. Sci Technol Weld Join 17:649–655. https://doi.org/10.1179/1362171812Y.0000000058

26. Huang YX, Han B, Tian Y et al (2011) New technique of filling friction stir welding. Sci Technol Weld Join 16:497–501. https://doi.org/10.1179/1362171811Y.0000000032

27. Miles MP, Feng Z, Kohkonen K et al (2010) Spot joining of AA 5754 and high strength steel sheets by consumable bit. Sci Technol Weld Join 15:325–330. https://doi.org/10.1179/136217110X12707333260491

28. Li WY, Fu T, Hütsch L et al (2014) Effects of tool rotational and welding speed on microstructure and mechanical properties of bobbin-tool friction-stir welded Mg AZ31. Mater Des 64:714–720. https://doi.org/10.1016/j.matdes.2014.07.023

29. Chen J, Fujii H, Sun Y et al (2017) Optimization of mechanical properties of fine-grained non-combustive magnesium alloy joint by asymmetrical double-sided friction stir welding. J Mater Process Technol 242:117–125. https://doi.org/10.1016/j.jmatprotec.2016.11.021

30. Niu S, Wu B, Ma L, Lv Z, Yan D (2018) Passive filling friction stir repairing AZ31-B magnesium alloy by external stationary shoulder. Int J Adv Manuf Technol 97:2461–2468. https://doi.org/10.1007/s00170-018-2130-7

Publisher's note Springer Nature remains neutral with regard to jurisdictional claims in published maps and institutional affiliations.